Agricultural and Forest Meteorology 390 (2026) 111486

Contents lists available at ScienceDirect

Agricultural and Forest Meteorology

journal homepage: www.elsevier.com/locate/agrformet

A semi-analytical Robin boundary extension for the infinite line source model that accounts for convective heat transfer in heat-pulse measurements

Tianyue Zhao [a], Yili Lu [a,b,*], Robert Horton [c], Tusheng Ren [a]

[a] College of Land Science and Technology, China Agricultural University, Beijing, 100193, China
[b] Key Laboratory of Arable Land Conservation in North China, Ministry of Agriculture and Rural Affairs, Beijing, 100193, China
[c] Department of Agronomy, Iowa State University, Ames, IA, 50011, USA

ARTICLE INFO

Keywords:
Heat-pulse method
Near-surface soil
Soil thermal property
Robin boundary condition
Soil-atmosphere interface
Analytical solution

ABSTRACT

Accurate determination of near-surface soil thermal property values with the heat-pulse (HP) method is essential to quantify energy and mass transfer across the soil-atmosphere interface. However, heat exchange at this interface is bound to violate the underlying adiabatic or isothermal boundary assumptions of the HP method. This study overcomes this limitation by using a Robin (third-kind) boundary condition instead of a zero-flux boundary condition in the infinite line source (ILS) model, hereafter termed ILS-RBC. A surface apparent heat transfer coefficient (h) is used to quantify boundary heat exchange. The performances of the ILS model, the adiabatic extension (ILS-ABC), and the ILS-RBC model were evaluated using finite-element simulations and wind-tunnel experiments across a range of surface heat transfer intensities and sensor depths (z). The ILS-RBC model accurately reproduced non-adiabatic near-surface temperature responses, with simulated HP signals matching observations closely (RMSE < 0.017°C). In contrast, the ILS and ILS-ABC models exhibited substantial biases that varied systematically with h and sensor depth, with thermal conductivity (λ) showing the greatest sensitivity. At $z = 1$ mm, as h increased from 0 to 20 W m^{-2} K^{-1}, λ estimates from the ILS and ILS-ABC models deviated by over 29%, while the ILS-RBC model kept variations within 2% and errors below 3%. The ILS-RBC model provides a theoretical representation considering non-adiabatic convection conditions for near-surface HP measurements.

1. Introduction

Accurate determinations of near-surface soil thermophysical property values are essential to quantify soil temperature dynamics, the surface energy balance, and evapotranspiration, and to improve land-surface parameterizations (Peters-Lidard et al., 1998; Vanderborght et al., 2017). Unlike subsurface soil layers, the thermal regime of near-surface soils is closely linked to atmospheric conditions, with intense and rapidly changing heat and mass exchange at the soil-atmosphere boundary. As a result, heat transfer in these layers depends on both internal conduction and active exchange across the interface. (Philip and Kluitenberg, 1999; Sakai et al., 2011). Accurate estimation of soil thermal property values within this boundary-affected region therefore remains challenging.

The heat-pulse (HP) technique, which enables rapid, in situ, and simultaneous measurement of multiple thermal properties in near-surface soil layers, has been widely used for field determination of soil water evaporation, surface heat flux, and energy balance (Ochsner et al., 2007; Heitman et al., 2008, 2017; He et al., 2018; Lu et al., 2025). Its underlying analytical framework relies on the infinite line source (ILS) model, which is derived under the assumption of a homogeneous, isotropic, and infinite medium (de Vries, 1963; Kluitenberg et al., 1993; Bristow et al., 1994). This framework performs well when HP sensors are placed sufficiently deep in soil, where boundary interference is negligible. With the increasing demand for near-surface observations, the distance between sensor location and soil surface has been progressively decreased (Heitman et al., 2008;Heitman et al., 2017; Li et al., 2025), which may severely violate the assumption of an infinite medium around the sensor (Philip and Kluitenberg, 1999; Xiao et al., 2015). It has been found that at shallow depths, the soil-atmosphere interface may significantly alter the propagation path, peak temperature rise, and attenuation characteristics of the HP (Liu et al., 2013; Peng et al., 2024).

* Corresponding author at: College of Land Science and Technology, China Agricultural University, Beijing, 100193, China.
E-mail address: luyili@cau.edu.cn (Y. Lu).

https://doi.org/10.1016/j.agrformet.2026.111486
Received 23 April 2026; Received in revised form 24 August 2026; Accepted 14 September 2026
Available online 22 September 2026
0168-1923/© 2026 Elsevier B.V. All rights are reserved, including those for text and data mining, AI training, and similar technologies.

There exists a need to develop new mathematical solutions for interpreting HP measured data near the soil-atmosphere boundary.

To mitigate biases caused by near-surface boundary effects, Liu et al. (2013) extended the ILS model by introducing the adiabatic boundary condition (ILS-ABC), which treats the soil as a semi-infinite medium with a zero-heat-flux upper boundary. While the adiabatic boundary assumption marks an extension of the HP model from an "infinite medium" to a near-surface bounded domain, it remains overly idealized and simplistic for many field conditions. By assuming a zero-heat flux, the ILS-ABC model neglects heat exchange between the soil surface and the atmosphere. Under conditions with strong airflow disturbance, wind-driven convective heat transfer may significantly enhance heat exchange at the soil surface, thereby violating the adiabatic assumption and introducing substantial estimation biases (Sang et al., 2020). A theoretical framework that explicitly characterizes non-adiabatic heat exchange at the soil-atmosphere interface is therefore required.

To address this limitation, we develop a semi-analytical model that includes a Robin (third-kind) boundary condition to analyze near-surface HP measurements. This study aims to systematically investigate the effects of interfacial heat exchange under convection conditions on temperature responses and thermal property estimation by explicitly accounting for the apparent heat transfer coefficient (h) at the soil surface. We further test the newly developed model via numerical simulations and controlled wind-tunnel experiments on dry sand.

2. Materials and methods

2.1. Semi-analytical solution for the ILS-RBC model

The heating needle of a buried HP sensor is commonly approximated as an infinite line heat source oriented parallel to the soil surface. To derive the new model, a two-dimensional Cartesian coordinate system is defined (Fig. 1), in which the soil-atmosphere interface is located at $x = 0$ ($x > 0$ denotes the soil domain), and a buried needle extends infinitely in the direction perpendicular to the xy-plane. The heating needle (H_1) is idealized as a two-dimensional instantaneous point-source located at (x_1, y_1), whereas the temperature sensor (S) is located at (x_2, y_2). The two-dimensional transient heat conduction process is governed by the following linear partial differential equation:

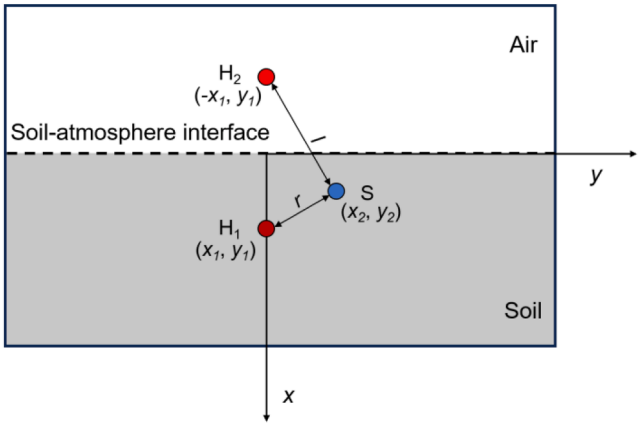

Fig. 1. Schematic diagram showing needle positions in the defined Cartesian coordinate system. H_1 and H_2 represent the heating needle in the soil and the image (the mirrored image of the actual heat source reflected across the soil-atmosphere interface) heat source in the air, respectively. S denotes the temperature sensor at an arbitrary position. r is the distance between H_1 and S, and l is the distance between H_2 and S.

$$\frac{\partial T}{\partial t} = \alpha\left(\frac{\partial^2 T}{\partial x^2} + \frac{\partial^2 T}{\partial y^2}\right) \tag{1}$$

where α is soil thermal diffusivity ($m^2\ s^{-1}$).

To represent heat transfer from a HP sensor placed at a shallow soil depth, we developed a semi-analytical model, ILS-RBC, which extends the traditional infinite line source (ILS) framework by incorporating a Robin (third-kind) boundary condition. Based on Newton's law of cooling, this Robin boundary condition at the soil-atmosphere interface ($x = 0$) is expressed as (Carslaw and Jaeger, 1959):

$$-\lambda \left.\frac{\partial T}{\partial x}\right|_{x=0} = h(T_s - T_a) \tag{2}$$

where T_s is soil surface temperature, T_a is the air temperature at a reference height above the soil surface, λ is soil thermal conductivity ($W\ m^{-1}\ K^{-1}$), and h is the apparent heat transfer coefficient ($W\ m^{-2}\ K^{-1}$), which represents the combined effects of sensible, latent, and radiative heat exchange across the soil-atmosphere interface. This formulation assumes linear boundary heat exchange and a constant h during each HP measurement. It should be noted that the reference height for T_a must be the same as the evaluation height of h.

The Green's function method (Ozisik, 1989) is used to derive the spatiotemporal response of the system to a heat pulse in a two-dimensional cross-section. By the product theorem (Newman, 1936), the Green's function for an instantaneous source in a two-dimensional temperature field, G_{xy}, can be expressed as the product of two independent one-dimensional components:

$$G_{xy}(x_2, y_2, t|x_1, y_1) = G_x(x_2, t|x_1) \times G_y(y_2, t|y_1) \tag{3}$$

where G_x represents one-dimensional conduction along the x-axis in a semi-infinite medium, and G_y represents one-dimensional conduction along the y-axis in an infinite medium.

At $t = 0$, for an instantaneous plane heat source located at $y = y_1$, the corresponding one-dimensional Green's function is given by:

$$G_y(y_2, t|y_1) = \frac{1}{\sqrt{4\pi\alpha t}} \exp\left(-\frac{(y_2 - y_1)^2}{4\alpha t}\right) \tag{4}$$

In the x-direction, the one-dimensional Green's function subject to the Robin boundary condition (Eq. [3]) is obtained by Laplace transformation (Carslaw and Jaeger, 1959):

$$\begin{aligned} G_x(x_2, t|x_1) = {} & \frac{1}{2\sqrt{\pi\alpha t}}\left[\exp\left(-\frac{(x_2 - x_1)^2}{4\alpha t}\right) + \exp\left(-\frac{(x_2 + x_1)^2}{4\alpha t}\right)\right] \\ & -\frac{h}{\lambda}\exp\left(\frac{\alpha t h^2}{\lambda^2} + \frac{h(x_2 + x_1)}{\lambda}\right)\operatorname{erfc}\left(\frac{x_2 + x_1}{2\sqrt{\alpha t}} + \frac{h\sqrt{\alpha t}}{\lambda}\right) \end{aligned} \tag{5}$$

For practical applications, the heating needle is assumed to generate a HP with a constant line power q' over a duration of t_0, rather than an instantaneous heating. According to the principle of linear superposition, the analytical solution for the temperature response at the measurement point (x_2, y_2) can be obtained by integrating the source term over time:

$$T(x_2, y_2, t) = \frac{q'}{\rho c}\int_0^{t'} G_{xy}(x_2, y_2, t - \tau|x_1, y_1)\, d\tau \tag{6}$$

where ρc is soil volumetric heat capacity. The upper integration limit, t', depends on the observation stage: $t' = t$ during the heating phase

($0 < t \le t_0$), and $t' = t_0$ during the cooling phase ($t > t_0$).

Substituting Eqs. [3-5] into Eq. [6] yields the analytical expressions for the ILS-RBC model during the heating and cooling phases, respectively:

$$\Delta T(x_1,y_1,x_2,y_2,h,t) = -\frac{q'}{4\pi\lambda}Ei\left[-\frac{r^2}{4\alpha t}\right] - \frac{q'}{4\pi\lambda}Ei\left[-\frac{l^2}{4\alpha t}\right] - \frac{q'\alpha}{\lambda}\sqrt{\frac{1}{4\pi\alpha}}\frac{h}{\lambda}\int_0^t \frac{1}{\sqrt{\tau}}\exp\left(\frac{\alpha\tau h^2}{\lambda^2} + \frac{h(x_2+x_1)}{\lambda} - \frac{(y_2-y_1)^2}{4\alpha\tau}\right)\mathrm{erfc}\left(\frac{x_2+x_1}{2\sqrt{\alpha\tau}} + \frac{h\sqrt{\alpha\tau}}{\lambda}\right)d\tau \tag{7a}$$

$$\begin{aligned}\Delta T(x_1,y_1,x_2,y_2,h,t) = {} & \frac{q'}{4\pi\lambda}\left\{Ei\left[-\frac{r^2}{4\alpha(t-t_0)}\right] - Ei\left[-\frac{r^2}{4\alpha t}\right]\right\} + \frac{q'}{4\pi\lambda}\left\{Ei\left[-\frac{l^2}{4\alpha(t-t_0)}\right] - Ei\left[-\frac{l^2}{4\alpha t}\right]\right\} \\ & -\frac{q'\alpha}{\lambda}\sqrt{\frac{1}{4\pi\alpha}}\frac{h}{\lambda}\int_{t-t_0}^t \frac{1}{\sqrt{\tau}}\exp\left(\frac{\alpha\tau h^2}{\lambda^2} + \frac{h(x_2+x_1)}{\lambda} - \frac{(y_2-y_1)^2}{4\alpha\tau}\right)\mathrm{erfc}\left(\frac{x_2+x_1}{2\sqrt{\alpha\tau}} + \frac{h\sqrt{\alpha\tau}}{\lambda}\right)d\tau\end{aligned} \tag{7b}$$

The geometric distances from the temperature sensor to the real heat source (r) and its image (the mirrored image of the actual heat source reflected across the soil-atmosphere interface) source (l) are determined from the coordinates of H_1, H_2, and S:

$$r = \sqrt{(x_2-x_1)^2 + (y_2-y_1)^2} \tag{8}$$

$$l = \sqrt{(x_1+x_2)^2 + (y_2-y_1)^2} \tag{9}$$

From Eq. [7], the analytical expression for the ILS-RBC model involves a complex nonlinear combination of the complementary error function (*erfc*) and exponential terms, making it difficult to obtain an explicit closed-form solution for the time integral. Therefore, in the parameter estimation procedure, the Gauss-Kronrod quadrature rule (Piessens et al., 1983;) is applied to achieve high-precision numerical integration. Subsequently, soil thermal properties are estimated by fitting the ILS-RBC model to the measured temperature rise (ΔT) versus time data using the Nelder-Mead simplex algorithm (Nelder and Mead, 1965).

2.2. Conceptual framework for the new model

The traditional infinite line source (ILS) model assumes an infinite, isotropic, and homogeneous soil medium with a uniform initial temperature distribution. Building upon this theoretical framework, de Vries (1952) derived a specific solution that accounts for a finite heating duration, thereby adapting the ILS model to HP sensor measurements. For $t > t_0$, when the heating needle releases heat for a duration of t_0 at a heat input per unit length of q' (W m^{-1}), the temperature rise (ΔT) at a radial distance r from the heat source can be expressed as follows:

$$\Delta T(r,t) = \frac{q'}{4\pi\lambda}\left\{Ei\left[\frac{-r^2}{4\alpha(t-t_0)}\right] - Ei\left[\frac{-r^2}{4\alpha t}\right]\right\} \tag{10}$$

where $Ei(-x)$ is the exponential integral, and t is the elapsed time since the onset of heating (s).

To address limitations of the infinite-medium assumption of the ILS model near the soil surface, Liu et al. (2013) presented the adiabatic boundary condition model (ILS-ABC). Based on the method of images (Philip and Kluitenberg, 1999), this model approximates the soil-atmosphere interface as an adiabatic boundary condition (ABC). For $t > t_0$, ΔT values calculated by the ILS-ABC model are given by:

$$\begin{aligned}\Delta T(r,l,t) = {} & \frac{q'}{4\pi\lambda}\left\{Ei\left[\frac{-r^2}{4\alpha(t-t_0)}\right] - Ei\left[\frac{-r^2}{4\alpha t}\right]\right\} \\ & + \frac{q'}{4\pi\lambda}\left\{Ei\left[\frac{-l^2}{4\alpha(t-t_0)}\right] - Ei\left[\frac{-l^2}{4\alpha t}\right]\right\}\end{aligned} \tag{11}$$

where l is the radial distance between the measurement point and the virtual (image) heat source.

Under field or other non-ideal experimental conditions, the soil surface heat fluxes are continuously affected by wind disturbance and soil-atmosphere water vapor exchange, thereby invalidating the adiabatic boundary assumption (Sang et al., 2020). To overcome this limitation, the ILS-RBC model modifies the upper boundary condition (Eq. [2]) to account for these complex heat fluxes. Fig. 2 shows the

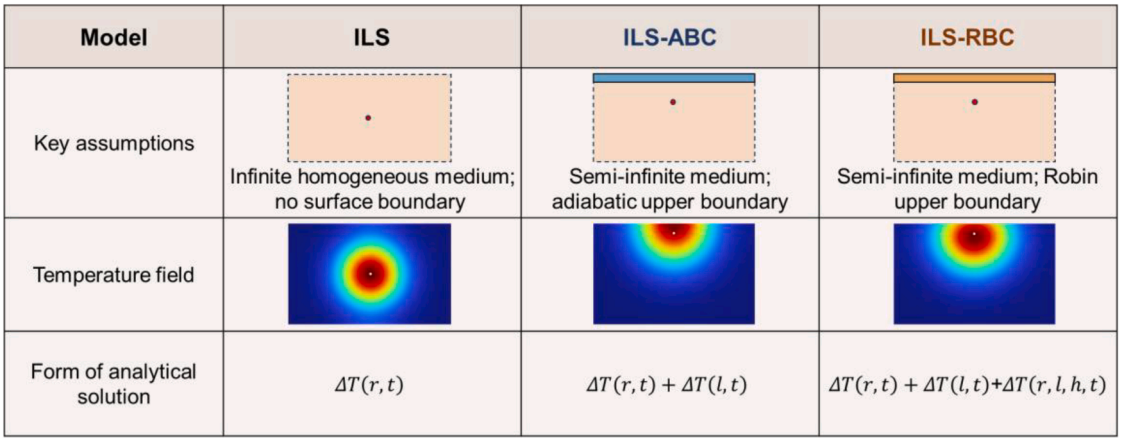

Fig. 2. Comparisons of the ILS, ILS-ABC, and ILS-RBC models in terms of upper boundary assumptions, transient temperature distributions, and the composition of their analytical expressions.

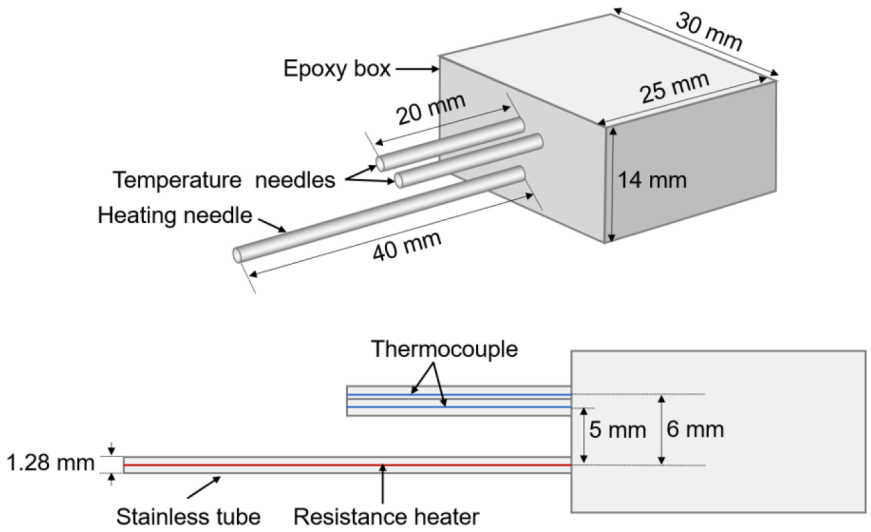

Fig. 3. Schematic view of the custom-made multi-needle heat pulse sensor.

comparisons between the proposed new model and traditional models in terms of their physical frameworks, boundary constraints, and transient temperature distributions. This comparison highlights the theoretical benefits of the ILS-RBC model. Unlike the ILS model, it can be used for near-surface layers, and unlike the ILS-ABC model, it explicitly considers interfacial heat loss. As a generalized framework, the ILS-RBC model reduces mathematically to the ILS-ABC model under an ideal adiabatic boundary condition ($h = 0$) and asymptotically approaches the traditional ILS model at sufficient soil depths where surface-boundary effects become negligible (Text S1). Consequently, it provides a rigorous and unified approach to accurately estimate near-surface soil thermal property values.

2.3. Laboratory wind-tunnel experiments

Laboratory experiments were performed using dry sand (98% sand and 2% silt) to study the effects of near-surface air disturbances on HP measurements. Soil samples were passed through a 2-mm sieve, oven-dried at 105°C for 24 h, and then packed in layers into cylindrical Plexiglass containers (12 cm in diameter and 10 cm in height) at a target bulk density (ρ) of 1.65 g cm^{-3}. The specific heat capacity (c) of the sand was 751 J kg^{-1} K^{-1}, which was determined using a differential scanning calorimeter (200F3 DSC, Netzsch-Geratebau GmbH, Selb, Germany).

For HP measurements, we used a custom-made three-needle sensor (Fig. 3). Each needle consisted of a stainless-steel tube with an outer diameter of 1.28 mm and an inner diameter of 0.84 mm. One needle served as the heating needle (40 mm long, containing a 75-μm-diameter Nichrome wire with a resistance of 222 Ω m^{-1}), whereas the other two needles served as temperature needles (20 mm long, containing E-type thermocouples). The horizontal spacing between the heating needle and the temperature needles was 6 mm, and the vertical spacing between the two temperature needles was 1 mm. During the experiments, the HP sensor was fixed within the soil column. The heating needle was installed at a depth of 7 mm, and the corresponding temperature needles were positioned at depths of 1 and 2 mm, respectively. Data were acquired using a CR3000 datalogger (Model CR3000, Campbell Scientific, Logan, USA) at a sampling frequency of 1 Hz. The t_0 was set to 8 s, with background temperature recorded for 60 s prior to the heat pulse and the heating response monitored for 120 s.

To simulate the effects of near-surface air disturbances on HP measurements, an axial fan was used to generate stable airflow over the soil column (Fig. 4). Wind speed (v) was monitored in real time using a hot-wire anemometer positioned 2 cm above the soil surface. Three wind-speed levels were investigated: $v = 0$, 1.5, and 3.5 m s^{-1}, with the airflow directed perpendicular to the sensor planes. Each treatment was performed in triplicate. Before each heating event, background room temperature was recorded for 60 s, and measurements were initiated only when temperature fluctuations were <0.03°C to minimize the influence of ambient temperature drift.

Physically, the apparent heat transfer coefficient encompasses multiple interfacial energy exchange processes, including sensible heat convection, latent heat of evaporation, and net radiation (Carslaw and Jaeger, 1959). Under the conditions of this study, the interference of latent heat flux and radiative heat transfer was assumed to be negligible

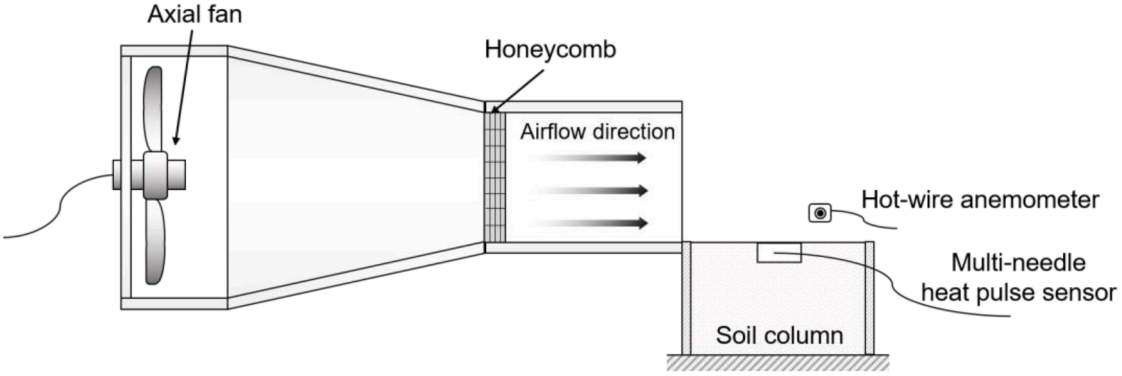

Fig. 4. Schematic diagram of the laboratory wind-tunnel experiment setup.

because the sample was dry sand and there was no direct solar radiation. Thus, the main factor affecting HP measurements was the convective heat transfer at the soil-atmosphere interface due to wind flow. For this reason, the soil-atmosphere interface was assumed to act as a flat plate with a laminar boundary layer. Thus, h can be calculated using the classical empirical heat-transfer correlation based on the Nusselt number (Nu) (Whitaker, 1972):

$$Nu = \frac{hL}{\lambda_a} = 0.664 Re^{0.5} Pr^{0.33} \tag{12}$$

where Re is the Reynolds number, and Pr is the Prandtl number, defined as follows:

$$Re = \frac{\rho_a v L}{\mu_a} \tag{13}$$

$$Pr = \frac{\mu_a c_a}{\lambda_a} \tag{14}$$

where L represents the characteristic length of the flow direction, and v is the designated wind speed (m s^{-1}). In the experiment, airflow passed horizontally over the exposed soil surface, and the soil column diameter was used as the characteristic length in the flow direction for estimating h. The thermophysical properties of air at standard atmospheric pressure and a constant room temperature of 17°C are: thermal conductivity $\lambda_a = 0.025$ W m^{-1} K^{-1}, density $\rho_a = 1.22$ kg m^{-3}, dynamic viscosity $\mu_a = 18.0$ μPa s, and constant-pressure specific heat $c_a = 1.0$ kJ kg^{-1} K^{-1} (Lemmon et al., 2013).

Substituting Eqs. [13] and [14] into Eq. [12] yields a direct relationship between h and wind speed v:

$$h = 0.664 \frac{\lambda_a}{L} \left(\frac{\rho_a v L}{\mu_a}\right)^{0.5} \left(\frac{\mu_a c_a}{\lambda_a}\right)^{0.33} \tag{15}$$

It should be emphasized that Eq. [15] is only applicable to determine the apparent heat transfer coefficient for wind-driven convection heat transfer. For the presented experimental conditions, both latent and radiative heat exchanges at the soil-atmosphere interface were neglected.

2.4. Numerical simulation

Finite-element simulations were performed using COMSOL Multiphysics (Version 6.0, COMSOL, Inc., Burlington, USA) to evaluate the accuracy of the ILS-RBC model. A two-dimensional geometric model with a uniform initial temperature of 17°C was used (Fig. 5). To satisfy the infinite line source assumption of the analytical model, the heating needle was treated as an ideal line heat source in the two-dimensional domain, and the thermophysical properties of the probe materials were neglected. The soil parameters used in the simulations were set equal to the reference values determined from laboratory measurements ($\lambda = 0.25$ W m^{-1} K^{-1}, $\alpha = 2.02 \times 10^{-7}$ m^2 s^{-1}, $c = 751$ J kg^{-1} K^{-1}, and $\rho = 1.65$ g cm^{-3}), with $q' = 46.5$ W m^{-1} and $t_0 = 8$ s. The upper boundary of the computational domain (the soil-atmosphere interface) was defined as a Robin boundary condition, with values of 0, 5, 10, 15, 20, 25, or 30 W m^{-2} K^{-1} assigned to h. All other boundaries were specified to be adiabatic.

2.5. Error analysis

Relative error (RE) was used to evaluate the accuracy of three models (ILS-RBC, ILS-ABC, and ILS) to estimate soil thermal properties (λ, α, ρc):

$$\mathrm{RE} = \frac{x_m - x_0}{x_0} \times 100 \tag{16}$$

where x_m is the thermal property value estimated by the model, and x_0 is the corresponding reference value. In this study, the reference values are: $\lambda_0 = 0.25$ W m^{-1} K^{-1}, $\alpha_0 = 2.02 \times 10^{-7}$ m^2 s^{-1} and $c_0 = 751$ J kg^{-1} K^{-1}.

To further evaluate the agreement between the modeled and reference temperature responses, the root mean square error (RMSE) and mean absolute error (MAE) were calculated:

$$\mathrm{RMSE} = \sqrt{\frac{1}{n}\sum_{i=1}^{n}\left(T_{m,i} - T_{o,i}\right)^2} \tag{17}$$

$$\mathrm{MAE} = \frac{1}{n}\sum_{i=1}^{n}\left|T_{m,i} - T_{o,i}\right| \tag{18}$$

where $T_{m,i}$ and $T_{o,i}$ represent the modeled and reference temperature values, respectively, and n is the number of temperature observations.

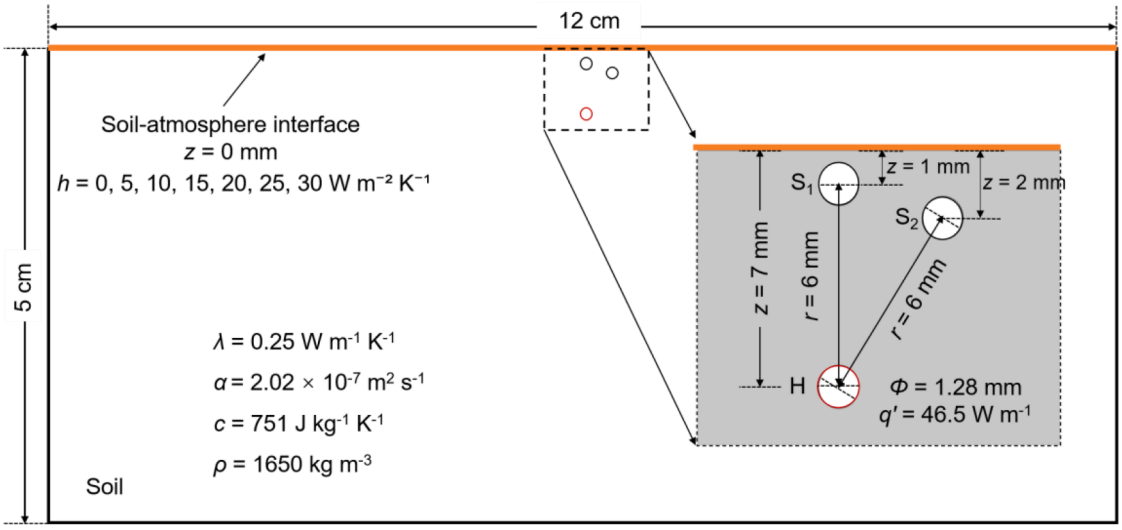

Fig. 5. Geometric configuration and simulation parameters for the finite-element model. H denotes the heating needle (heat input q' and the heating duration t_0), and S_1 and S_2 indicate the temperature needles at specified sensor depths z. The rectangular soil domain (12 cm in length and 5 cm in depth) is assigned uniform values of soil thermal conductivity λ, thermal diffusivity α, specific heat capacity c, and soil bulk density ρ. For the upper boundary condition (the soil-atmosphere interface, the orange line), a variety of values were assigned to the apparent heat transfer coefficient h.

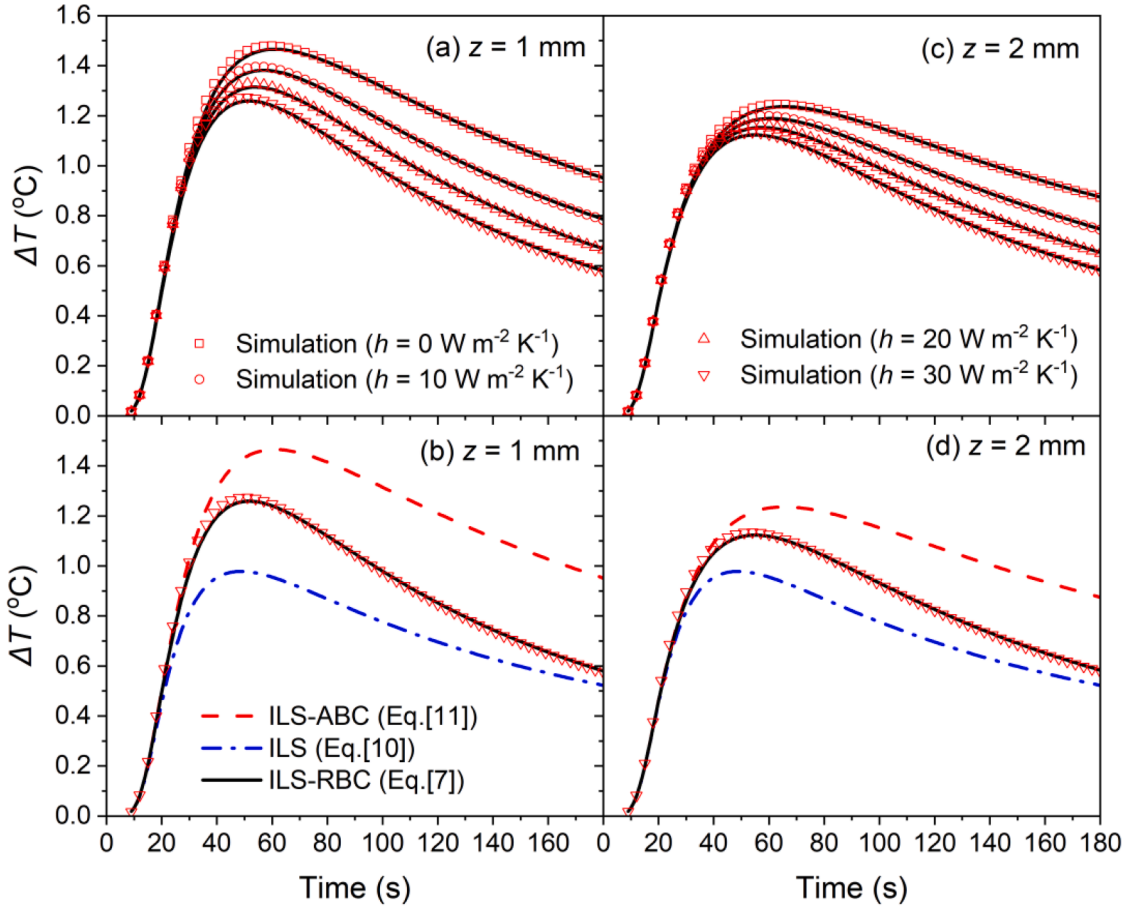

Fig. 6. Comparison of temperature with time response curves between the ILS-RBC model and numerical simulations in dry sand for various apparent heat transfer coefficient values (h) at sensor depths of (a) $z = 1$ mm and (c) $z = 2$ mm, and the ILS, ILS-ABC, and ILS-RBC models at $h = 30$ W m^{-2} K^{-1} for (b) $z = 1$ mm and (d) $z = 2$ mm.

3. Results and discussion

3.1. Comparison of modeled and simulated temperature rise versus time

To verify the accuracy of the semi-analytical solution (ILS-RBC model) presented in Section 2.2, a two-dimensional heat transfer model was constructed in COMSOL Multiphysics using the same physical parameters and boundary conditions. Fig. 6 shows the temperature-time curves obtained from the semi-analytical solution and the numerical simulations for scenarios of different sensor depths ($z = 1$ and 2 mm) and h values. There is excellent agreement between the temperature response curves generated by the two approaches, with $R^2 > 0.99$, an RMSE of <0.017°C, and an MAE of <0.016°C for the HP measurement period (9–180 s). This indicates that the ILS-RBC model enables to reproduce heat transfer behavior of HP measurement under non-adiabatic boundary conditions.

The effect of h values on temperature responses was illustrated at 1-mm and 2-mm sensor depths, respectively (Figs. 6a, 6c). Under non-adiabatic surface boundary conditions, as h increased, the enhanced interfacial heat loss at the soil-atmosphere boundary attenuated the temperature response, manifested as reduced peak temperature rise (ΔT_m) and earlier time to peak (t_m). At $z = 1$ mm, ΔT_m decreased from 1.48°C under adiabatic conditions ($h = 0$ W m^{-2} K^{-1}) to 1.27°C at $h = 30$ W m^{-2} K^{-1}, with t_m occurring 9 s earlier. Similarly, at $z = 2$ mm, increasing h from 0 to 30 W m^{-2} K^{-1} reduced ΔT_m from 1.25°C to 1.13°C, and advanced t_m by about 11 s. These results demonstrate that the magnitude of interfacial heat exchange effects depends strongly on measurement depth. Comparisons were also made between the HP temperature responses predicted by the ILS-RBC, ILS-ABC, and ILS models for the same prescribed soil thermal property values and sensor configuration (Figs. 6b, 6d). For the representative non-adiabatic condition, the ILS-RBC response closely matched the finite-element simulated values, whereas the ILS-ABC and ILS models significantly overestimated and underestimated the temperature responses, respectively, especially for the after-peak measurement period. Earlier finite-element studies examined near-surface HP responses under adiabatic boundary assumptions (Sang et al., 2020; Peng et al., 2024). This current investigation suggests that ignoring a Robin boundary condition can lead to large errors in the simulated HP temperature responses. Overall, the close agreement between the ILS-RBC predictions and the finite-element simulations under various non-adiabatic conditions supports the model's ability to represent near-surface HP temperature responses.

3.2. Soil thermal property values estimated by the ILS-RBC, ILS-ABC, and ILS models

Figure 7 presents the relative errors (REs) for soil thermal properties (λ, α, and ρc) estimated by the ILS-RBC, ILS, and ILS-ABC models at sensor depths of $z = 1$ and 2 mm for seven apparent heat transfer coefficient levels ($h = 0$, 5, 10, 15, 20, 25, and 30 W m^{-2} K^{-1}). For these shallow needle depths, both the ILS and ILS-ABC models exhibited substantial systematic biases in estimating soil thermal property values, whereas the ILS-RBC model maintained high accuracy and stability. Under ideal adiabatic conditions ($h = 0$ W m^{-2} K^{-1}), the ILS-RBC and ILS-ABC models were equivalent; both gave relatively consistent results,

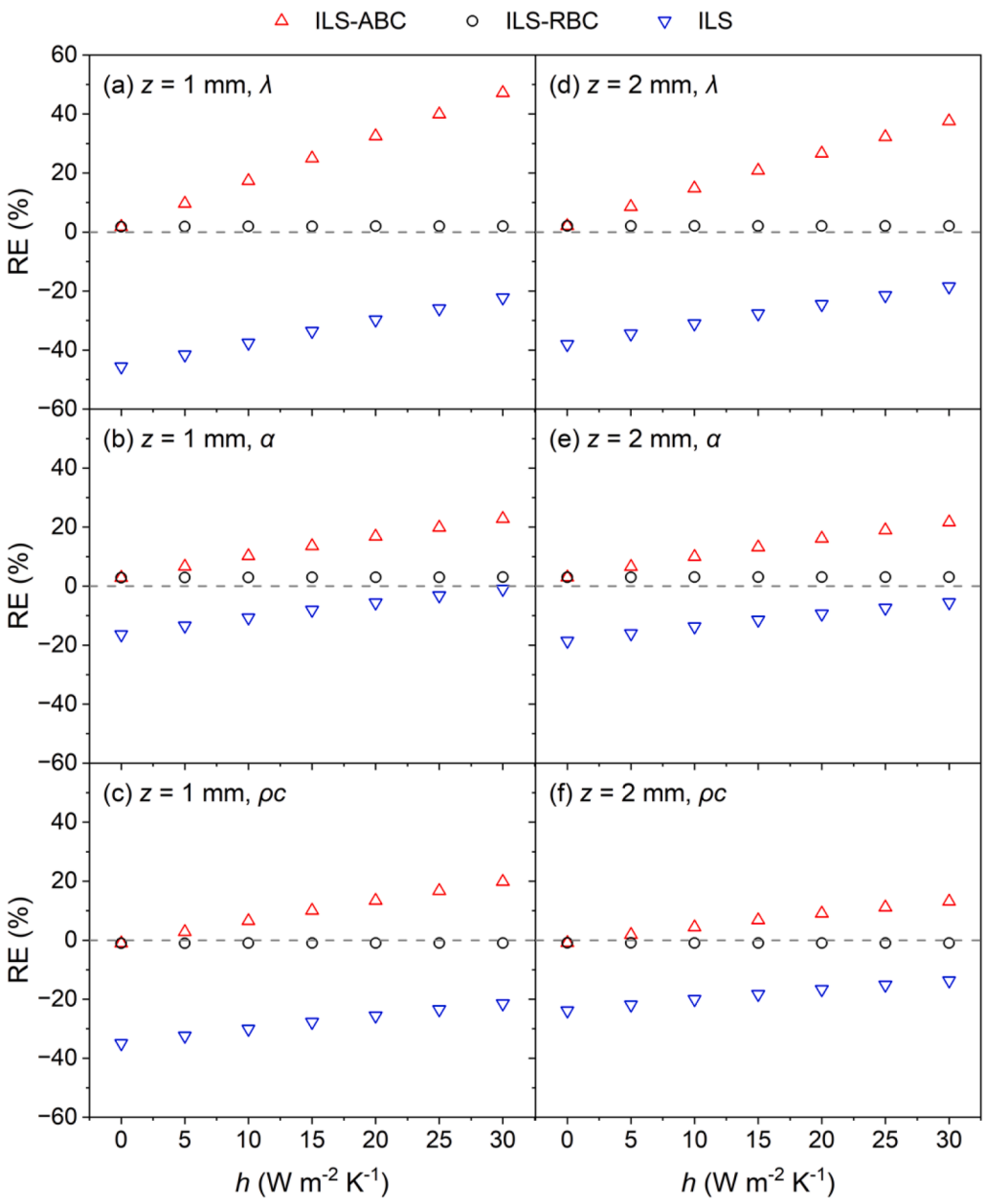

Fig. 7. Relative errors (REs) in the estimated soil thermal property values (λ, α, ρc) for dry sand obtained from the ILS-RBC, ILS, and ILS-ABC models under various values of apparent heat transfer coefficients ($h = 0$, 5, 10, 15, 20, 25, 30 W m^{-2} K^{-1}) and sensor depths ($z = 1$, 2 mm).

yielding errors below 3% in thermal property value estimations (Fig. 7). The ILS model that completely neglects the soil-atmosphere interface boundary produced substantially larger errors in λ, exceeding 16% and reaching up to 38%. It should be noted that the estimation errors in λ, α, and ρc varied almost linearly with h values. The ILS-ABC model with the adiabatic assumption resulted in larger errors with increasing h: at $z = 1$ mm and $h = 30$ W m^{-2} K^{-1}, the relative error in λ increased from 2% to 47%. While the ILS model severely underestimated thermal property values at $h = 0$ W m^{-2} K^{-1}, these errors appeared to decrease as h increased.

These conflicting biases arose because two primary heat transfer mechanisms occurred under such conditions: conduction within the soil and convection at the boundary. When convection heat transfer was minimal ($h = 0$), heat released by the sensor was mainly through soil conduction, allowing the ILS-ABC model to perform well since the boundary was effectively adiabatic. This heat buildup at the adiabatic boundary could cause significant errors in the ILS model (Sang et al., 2020). However, as h increased and convection became more prominent, the impact of heat accumulation near the surface diminished, leading to gradually decreasing errors for the ILS model. Overall, considering the third-kind boundary, the ILS-RBC model performed well for both adiabatic and non-adiabatic surface conditions by incorporating h to characterize interfacial heat flux. Across the evaluated range of h, the relative errors in estimated values of λ, α, and ρc remained stable with fluctuations below 1%, demonstrating a substantial reduction in systematic biases in estimates of the soil thermal property values induced by surface heat exchange.

3.3. Validation of the ILS-RBC model using wind-tunnel experiments

To validate the reliability of the ILS-RBC model, HP experiments were performed on homogeneous dry sand columns with a wind-tunnel device. Three distinct interfacial wind speeds were imposed across the soil-atmosphere interface: $v = 0$, 1.5, and 3.5 m s^{-1}. These conditions

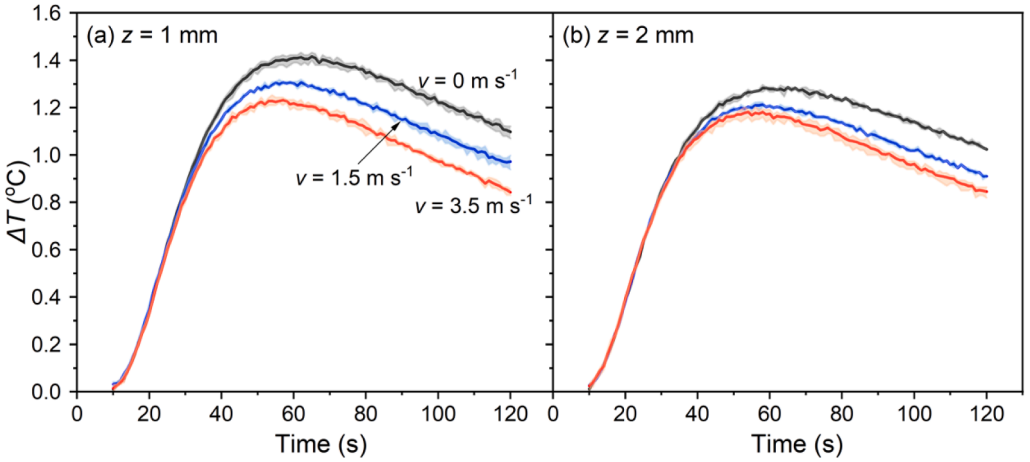

Fig. 8. Measured HP temperature response curves in dry sand under varying interfacial wind speeds (v): (a) sensor depth $z = 1$ mm; (b) sensor depth $z = 2$ mm. Solid lines represent the mean values of three replicates; shaded areas denote the observed range of values.

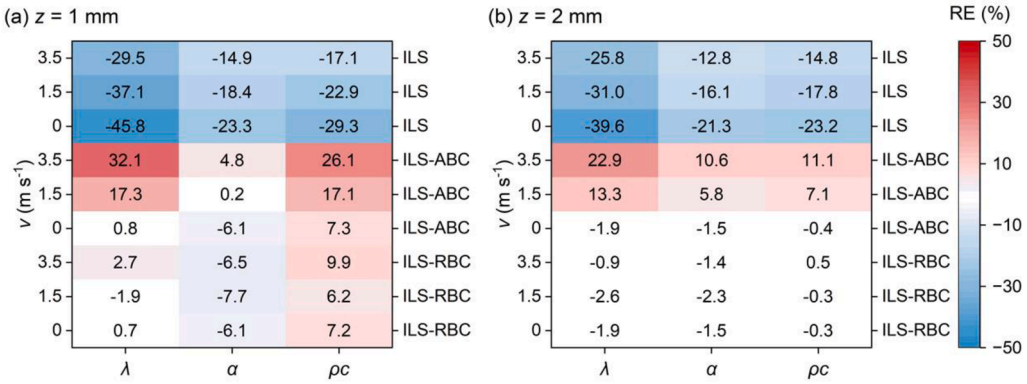

Fig. 9. Comparison of relative errors (REs) in the estimation of soil thermal property values (λ, α, ρc) for dry sand using the ILS, ILS-ABC, and ILS-RBC models. Results are shown for three interfacial wind speeds (v) and two sensor depths (z).

correspond to $h = 0$, 13.9, and 21.2 W m^{-2} K^{-1}, respectively, as calculated from Eq. [15].

Figure 8 presents the measured temperature-with-time response curves at two sensor depths under these boundary conditions. The observations confirm the fundamental patterns calculated by the numerical simulations: (1) the magnitude of ΔT_m values decreased with increasing wind speed, and (2) t_m occurred progressively earlier. Quantitatively, at a sensor depth of $z = 1$ mm, the measured ΔT_m values for the three wind speeds were 1.43, 1.32, and 1.25°C, respectively. At the highest wind speed ($v = 3.5$ m s^{-1}), t_m occurred 11 s earlier than under the no-wind condition ($v = 0$ m s^{-1}).

The observed responses are mechanistically consistent with enhanced interfacial energy exchange. Higher wind velocity intensifies convective heat transfer at the soil-atmosphere interface, leading to greater dissipation of the applied heat pulse energy to the atmosphere. Consequently, less thermal energy remains for conduction into the soil, which explains the decrease in ΔT_m and the earlier peak time (t_m). This validation confirms that the ILS-RBC model captures at least in part the coupling between surface boundary conditions (wind-driven convection) and soil heat transfer dynamics.

Figure 9 presents the REs in soil thermal property values estimated from the measured HP signals under varying interfacial wind conditions (detailed numerical results are presented in Appendix Tables S1–3). The performances of the three models applied to observed values align closely with the simulation trends presented in Fig. 7.

The ILS model exhibited significant systematic underestimation of all thermal property values. For example, at a sensor depth of $z = 1$ mm, the REs for λ, α, and ρc ranged from 30% to 46%, 15% to 23%, and 17% to 29%, respectively. Even at $z = 2$ mm, errors remained substantial (13% to 40%). These results confirm the violation of the infinite homogeneous medium assumption for near-surface soil conditions. The physical basis of this violation lies in the disruption of spatial symmetry of the HP sensor-generated temperatures by the soil-atmosphere interface. The strong thermophysical contrast between soil and air causes interface heat loss, which distorts the temperature field from an idealized isotropic evolution.

The ILS-ABC model generally outperformed the ILS model, except for the most severe convective condition ($z = 1$ mm, $v = 3.5$ m s^{-1}). Under quiescent conditions ($v = 0$ m s^{-1}), the ILS-ABC model estimated λ values with a minimum error of 1%. However, as wind speed increased to 1.5 and 3.5 m s^{-1}, the errors in λ rose sharply to 17% and 32%, respectively, with corresponding increases in ρc value errors to 17% and 26%, respectively. A similar trend, though with reduced magnitudes, was observed at $z = 2$ mm. These patterns demonstrate that the adiabatic boundary condition is valid only when interfacial heat exchange is negligible. As aerodynamic forcing intensifies (with increasing h), the adiabatic boundary assumption fails because it neglects actual cross-boundary energy flux. Consequently, the model incorrectly attributes this heat loss to apparent changes in soil thermal property values, creating a systematic bias that escalates with wind speed.

In contrast, the ILS-RBC model achieved the highest accuracy and stability under all experimental conditions. At $z = 1$ mm, REs for λ, α, and ρc were constrained to 1% to 3%, 6% to 8%, and 6% to 10%, respectively. At $z = 2$ mm, errors decreased further to within 3%. This

superior performance confirms that the improvement offered by the ILS-RBC model is not merely an empirical adjustment but stems from its physically rigorous representation of interfacial heat exchange. By explicitly accounting for the convective boundary condition, the model extends reliable thermal property estimation to near-surface environments where traditional approaches fail.

Figure 8 also illustrates the theoretical convergence of the ILS-RBC and ILS-ABC models under ideal adiabatic boundary conditions ($v = 0$ m s^{-1}), where their REs values are nearly identical. As v increases, the thermal properties exhibit differential sensitivity to non-adiabatic boundary effects. Notably, in both the ILS and ILS-ABC models, the increase in RE for λ exceeds that for α and ρc, indicating that λ is the thermal property most sensitive to surface heat loss.

This differential sensitivity is mechanistically consistent with the distinct physical processes governing each thermal property. Non-adiabatic interfacial heat transfer primarily attenuates the amplitude of the temperature rise ΔT, with a secondary effect on the timing of the peak t_m. In HP signal analysis, α is predominantly governed by the temporal characteristics of the temperature response, i.e., it is strongly correlated with t_m (Bristow et al., 1994). Consequently, α remains relatively robust to heat loss under non-adiabatic conditions. In contrast, λ, which directly quantifies heat flux density, is highly sensitive to the absolute magnitude of ΔT.

The estimation error for ρc follows a trend similar to that of λ because it is derived from the fundamental relationship $\rho c = \lambda/\alpha$. Systematic biases in λ and α induced by boundary effects thus propagate directly into the calculation of ρc. This coupling explains why the error patterns for ρc mirror those of λ, rather than exhibiting independent behavior.

3.4. Practical considerations for near-surface soil thermal property estimation

For near-surface HP measurements, it is important to investigate the effect of the soil-atmosphere boundary on the HP measurement depth. Additional analyses were performed to determine how sensor depth and the specification of h values affected the estimated values of λ, α, and ρc. The influence of the surface boundary on HP temperature responses decreases with increasing sensor depth. Under specific experimental conditions and the sensor configuration of this study, when surface heat exchange was non-negligible, the ILS model tended to underestimate, whereas the ILS-ABC model overestimated soil thermal property values in the upper 8 mm of soil. Therefore, for the 0–8 mm soil layer, the ILS-RBC model is recommended for HP measurements (Fig. S1). It is important to note that accurate specification of h in the ILS-RBC model becomes especially important at near-surface depths during periods of intense surface heat exchange. The sensitivity analysis also shows that the estimated λ values are more sensitive to variations in h than are values of α and ρc (Fig. S2). These results indicate that shallow measurements are particularly sensitive to both the representation of surface heat exchange and the reliability of specifying h under field conditions.

Applying the ILS-RBC model in complex field environments requires careful consideration of several practical limitations. The current model assumes a constant h value over the entire HP measurement period, even though the boundary heat flux varies with transient changes in surface temperature. In real-world conditions, factors such as intermittent wind gusts, evaporation, or temporary shading from solar radiation can cause notable short-term changes in the surface energy balance. Therefore, model performance under dynamic boundary conditions warrants further empirical investigation. Furthermore, near-surface soil layers are particularly susceptible to pronounced diurnal temperature drift. Future research should focus on combining the background temperature drift correction algorithm with the ILS-RBC model to ensure accurate measurement results under field conditions.

4. Conclusions

This study extends the ILS framework for near-surface HP measurements by developing a semi-analytical model that incorporates a Robin (third-kind) boundary condition. The model explicitly accounts for interfacial heat exchange at the soil-atmosphere interface through an apparent heat transfer coefficient, allowing non-adiabatic boundary conditions to be represented within the proposed framework.

The new ILS-RBC model is evaluated using a finite-element evaluation method as well as laboratory-controlled experiments. The results show that the ILS-RBC model can accurately reproduce near-surface HP signals, and improve the estimation accuracy of shallow soil thermal properties under varying interfacial heat transfer regimes. In contrast, conventional models (ILS and ILS-ABC) introduce systematic biases in the estimated thermal properties because of their simplified surface boundary assumptions. These biases become more pronounced closer to the soil surface, with λ showing the greatest sensitivity to surface heat exchange. Wind-tunnel experiments further indicate that the ILS-RBC model maintains superior estimation stability across a range of wind speeds (0–3.5 m s^{-1}) and sensor depths (1–2 mm) under controlled dry sand conditions. Notably, at $z = 1$ mm and $v = 3.5$ m s^{-1}, neglecting surface heat exchange results in errors exceeding 30% in λ estimations.

These findings highlight the value of the ILS-RBC model for reliable near-surface thermal property value estimations, particularly for conditions when conventional boundary assumptions introduce substantial errors. Further field validations are required to assess its broader applicability.

CRediT authorship contribution statement

Tianyue Zhao: Writing – original draft, Methodology, Data curation, Conceptualization. **Yili Lu:** Writing – review & editing, Supervision, Funding acquisition, Conceptualization. **Robert Horton:** Writing – review & editing. **Tusheng Ren:** Writing – review & editing.

Declaration of competing interest

The authors declare that they have no known conflict of interest or personal relationships that could have appeared to influence the work reported in this paper.

Acknowledgements

This work was supported by the Natural Science Foundation of China (42307390), and USDA-NIFA Multi-State Project 5188.

Supplementary materials

Supplementary material associated with this article can be found, in the online version, at doi:10.1016/j.agrformet.2026.111486.

Data availability

The data that has been used is confidential.

References

Bristow, K.L., Horton, R., Kluitenberg, G.J., 1994. Measurement of soil thermal properties with a dual-probe heat-pulse technique. Soil. Sci. Soc. Am. J. 58, 1288–1294. https://doi.org/10.2136/sssaj1994.03615995005800050002x.

Carslaw, H.S., Jaeger, J.C., 1959. Conduction of Heat in Solids. Clarendon Press, Oxford.

de Vries, D.A., 1952. A nonstationary method for determining thermal conductivity of soil in situ. Soil Sci. 73, 83–90. https://doi.org/10.1097/00010694-195202000-00001.

de Vries, D.A., 1963. Thermal properties of soils. In: Van Wijk, W.R. (Ed.), Physics of Plant Environment. North-Holland Publ, Amsterdam, pp. 210–235.

He, H., Dyck, M.F., Horton, R., Ren, T., Bristow, K.L., Lv, J., Si, B., 2018. Development and application of the heat pulse method for soil physical measurements. Rev. Geophys. 56, 567–620. https://doi.org/10.1029/2017rg000584.

Heitman, J.L., Horton, R., Sauer, T.J., DeSutter, T.M., 2008. Sensible heat observations reveal soil-water evaporation dynamics. J. Hydrometeorol. 9, 165–171. https://doi.org/10.1175/2007jhm963.1.

Heitman, J.L., Zhang, X., Xiao, X., Ren, T., Horton, R., 2017. Advances in heat-pulse methods: measuring soil water evaporation with sensible heat balance. Methods Soil Anal 2, 0. https://doi.org/10.2136/msa2015.0029.

Kluitenberg, G.J., Ham, J.M., Bristow, K.L., 1993. Error analysis of the heat pulse method for measuring soil volumetric heat capacity. Soil. Sci. Soc. Am. J. 57, 1444–1451. https://doi.org/10.2136/sssaj1993.03615995005700060008x.

Lemmon, E.W., Huber, M.L., McLinden, M.O., 2013. NIST Standard Reference Database 23: Reference Fluid Thermodynamic and Transport Properties-REFPROP, Version 9.1. National Institute of Standards and Technology. Standard Reference Data Program, Gaithersburg, MD.

Li, L., Lu, Y., Liu, L., Xie, X., 2025. The spatial and temporal variability of soil-water evaporation as influenced by near-surface soil porosities. Agronomy 15, 2654. https://doi.org/10.3390/agronomy15112654.

Liu, G., Zhao, L.J., Wen, M.M., Chang, X.P., Hu, K.L., 2013. An adiabatic boundary condition solution for improved accuracy of heat-pulse measurement analysis near the soil-atmosphere interface. Soil. Sci. Soc. Am. J. 77, 422–426. https://doi.org/10.2136/sssaj2012.0187n.

Lu, Y., Liu, Y., Peng, W., Fu, Y., Ren, T., Heitman, J., Horton, R., 2025. Monitoring dynamic water content, bulk density, and heat and water fluxes in the critical zone with thermo-time domain reflectometry sensors. Vadose Zone J. 24, e20390. https://doi.org/10.1002/vzj2.20390.

Nelder, J.A., Mead, R., 1965. A simplex algorithm for function minimization. Comput. J. 7, 308–313. https://doi.org/10.1093/comjnl/7.4.308.

Newman, A.B., 1936. Heating and cooling rectangular and cylindrical solids. Ind. Eng. Chem. 28, 545–548. https://doi.org/10.1021/ie50317a010.

Ochsner, T.E., Sauer, T.J., Horton, R., 2007. Soil heat storage measurements in energy balance studies. Agron. J. 99, 311–319. https://doi.org/10.2134/agronj2005.0103S.

Özışık, M.N., 1989. Boundary Value Problems of Heat Conduction. Courier Corporation.

Peng, W., Lu, Y., Ren, T., Horton, R., 2024. An adiabatic boundary condition with cylindrical perfect conductors for improved approximations from heat-pulse measurement near the soil-atmosphere interface. Geoderma 448, 116951. https://doi.org/10.1016/j.geoderma.2024.116951.

Peters-Lidard, C.D., Blackburn, E., Liang, X., Wood, E.F., 1998. The effect of soil thermal conductivity parameterization on surface energy fluxes and temperatures. J. Atmos. Sci. 55, 1209–1224. https://doi.org/10.1175/1520-0469(1998)055<1209:TEOSTC>2.0.CO;2.

Philip, J.R., Kluitenberg, G.J., 1999. Errors of dual thermal probes due to soil heterogeneity across a plane interface. Soil. Sci. Soc. Am. J. 63, 1579–1585. https://doi.org/10.2136/sssaj1999.6361579x.

Piessens, R., de Doncker-Kapenga, E., Überhuber, C.W., Kahaner, D.K., 1983. Quadpack: A Subroutine Package for Automatic Integration. Springer.

Sakai, M., Jones, S.B., Tuller, M., 2011. Numerical evaluation of subsurface soil water evaporation derived from sensible heat balance. Water. Resour. Res. 47, W07542. https://doi.org/10.1029/2010WR009866.

Sang, Y.J., Liu, G., Horton, R., 2020. Wind effects on soil thermal properties measured by the dual-probe heat pulse method. Soil. Sci. Soc. Am. J. 84, 414–424. https://doi.org/10.1002/saj2.20041.

Vanderborght, J., Fetzer, T., Mosthaf, K., Smits, K.M., Helmig, R., 2017. Heat and water transport in soils and across the soil-atmosphere interface: 1. Theory and different model concepts. Water. Resour. Res. 53, 1057–1079. https://doi.org/10.1002/2016WR019982.

Whitaker, S., 1972. Forced convection heat transfer correlations for flow in pipes, past flat plates, single cylinders, single spheres, and for flow in packed beds and tube bundles. AIChE J. 18, 361–371. https://doi.org/10.1002/aic.690180219.

Xiao, X., Zhang, X., Ren, T., Horton, R., Heitman, J.L., 2015. Thermal property measurement errors with heat-pulse sensors positioned near a soil–air interface. Soil. Sci. Soc. Am. J. 79, 766–771. https://doi.org/10.2136/sssaj2014.12.0493n.